N89-21755

1988

NASA/ASEE SUMMER FACILITY FELLOWSHIP PROGRAM

MARSHALL SPACE FLIGHT CENTER
THE UNIVERSITY OF ALABAMA

THE KEYHOLE REGION IN VPPA WELDS

Prepared by:	Daniel W. Walsh Ph.D.
Academic Rank:	Associate Professor
University and Department:	California Polytechnic State University, San Luis Obispo Metallurgy and Materials Engineering
NASA/MSFC:	
Laboratory:	Materials & Processes
Division:	Process Engineering
Branch:	Metals Processes
MSFC Colleague:	Arthur C. Nunes Jr., Ph.D.
Date:	August 8, 1988
Contract No.:	NGT 01-002-099 The University of Alabama

ABSTRACT

Title: Physical Processes Associated With the Weld Keyhole; Weld Macrosegregation and Arc Character

Daniel W. Walsh Cal Poly San Luis Obispo

The morphology and properties of the Variable Polarity Plasma Arc (VPPA) weld composite zone are intimately related to the physical processes associated with the keyhole. This study examined the effects of microsegregation and transient weld stress on macrosegregation in the weld pool. In addition the electrical character of straight and reverse polarity portions of the arc cycle were characterized. The results of the former study indicate that alloy 2219 is weldable because large liquid volumes are available during latter stages of weld solidificcation. Strains in the pool region, acting in conjunction with weld microsegregation can produce macrosegregation great enough to produce radiographic contrast effects in welds. Mechanisms of surface copper enrichment were identified. The latter study has demonstrated that increased heat is delivered to workpieces if the reverse polarity proportion of the weld cycle is increased. Current in the straight polairty portion of the welding cycle increases as the reverse cycle proportion increases. Voltage during reverse polarity segments is large.

Acknowledgement

Thanks to all who made this summer experience worthwhile and enjoyable. Special thanks to Ernestine Cothran and Mike Freeman for a well run program, thanks to Billie Swinford and Missy for taking their turn to "watch" me this summer. The list of NASA and contractor empoloyees who deserve my thanks could form the nucelus of a third political party. Risking a sin of ommission, these people are Benji Swain, whose constant interest, and insight helped make this summer successful, Dave Newman, Jeff Ding, Carolyn Kurgan, Jeff Norris, Frank Zimmerman, Bill McGee, Wayne Owen, Chip Jones, Rick Underwood, the entire staff of X-ray (please forgive me, I know how many loops you all willingly jumped through for me), Terry Craig, Mr. Craig, Tim Tittsworth (missed your cow) Angie, Ann Whitaker, Ph.D. Paul Gill, Svelte Marty Marttinez, and Ronnie (three point land) Renfroe. Despite my efforts neither Ken Swaim (my electronics guru) or Sam Clark (diety of welding) have recognized that the PAC 10 is the power conference in the country. I would also like to thank Joe Bucher and Richard Venable for their help, and Tim Vaughn and Dan Drinnan for their helpful comments. A special thanks to Joe Montano and Wendell Deweese, their help was invaluable and much appreciated. Thanks to James Coston and Gretchen Perry for their efforts. Thanks to Ernie Bayless for his interest and comments. Thanks to the a.m. discussion group (Joe Gregory and Art Nunes) for caustic comment cathartic coffee. I would like to thank Bertha Gildon for her help through the summer and for typing this manuscript. Thanks to NASA ASEE for fostering this program. A special thanks to Art Nunes, the personification of the NASA colleague concept. His constant interest, ready insight, and friendship made this summer, as last, a rewarding experience. Finally thanks to my wife and family whose patience and perseverence made this summer work possible and whose expenses make it manditory.

INTRODUCTION AND OBJECTIVES

The physics associated with the VPPA process is interesting for three reasons. First, though more information is collected each day, the keyhole and pool are not well understood. Indeed the VPPA keyhole process has not been as well characterized as other keyhole processes. Second, fluid flow and heat transfer fix the distribution of microstructure and properties in the weld composite region. Finally fluid flow in the pool and static forces on the pool determine bead morphology. Fluid flow in the weld pool was the subject of intense study during the summer of 1987[1]. During this summer program, pool solidification, the electrical character of the arc, and the morphology of VPPA weld beads were investigated. The steady state keyhole in shown in Figure (1). Energy is transferred to the work via a heated plasma directed by the plasma torch. Much of the energy transfer is accomplished by convective mechanisms in the hot, directed efflux plasma and by radiation from an arc that is buried in the keyhole region. In VPPA welding, the arc polarity switches many times a second, but the work is principally anodic. The oxide film associated with Al 2219 is disrupted by the sputtering action of argon ions during the reverse polarity portion of the cycle, and the arc is stabilized. A majority of the heat transfer occurs at the leading edge of the keyhole, where the anode spot is located and the plasma is directed. In this location the liquid is thin, and the thickness uniform regardless of depth in the keyhole. Around the keyhole, until the longitudinal centerline is passed the fluid remains thin. The thickness is not as uniform, becoming slightly larger deeper in the keyhole. In the rear, a croissant shaped fluid pool exists.

Recent success in joining HP-9-4-30 spurred interest in identifying the portions at energy delivered to welds during the straight or reverse periods of the VPPA welding cycle. The character of the welding arc differs drastically during the straight and reverse polarity periods in the cycle. As a rule, voltage increases but current falls during reverse polarity. Two key items examined for effect on power production were cathode emission efficiency, and altered arc resistance.

Recently much effort has been directed towards discerning the nature of a linear x-ray indication found in production welds on the external tank. The indication parallels the welding direction, and mimics dangerous lack of fusion or cracks so well that it triggers a repair response. However, when repaired, no defect is found. Nunes and Ding[2] have identified the cause of the indication, but here-to-fore no mechanism of formation has been established. This program established that mechanism. In order to understand the arguments presented a knowledge of weld solidification is required.

Pertinent Solidification Theory

Weld solidification theory can be used to explain the amounts and distribution of constituents in Al-2219 VPPA weld microstructures.

Figure (2) depicts the Al-Cu system, in our range of interest. The nominal composition (Co) is marked as 6.3% Cu, representing nominal 2219. Under conditions of equilibrium, a liquid of Co begins to form solid at the intercept of Co with the liquidus line. The composition of the first solid to form is defined by the temperature at that intersection. With continued cooling the composition of both the solid and the remaining liquid adjust, by diffusion, so that at any temperature the entire solid volume has a composition defined by the intercept of the isotherm and the solidus, and the entire volume of the remaining liquid has a composition defined by the intercept of the isotherm and the liquidus. Clearly, the assumption of uniform composition in the phases implies that the diffusion distances are much less than

Egn. 1 $$\sqrt{D t_f}$$

where D is the limiting diffusion in the system, and tf is the solidification time. At any temperature, invoking mass conservation.

Egn. 2 $$F_s C_s + f_\ell C_\ell = C_o$$

thus

Fs = fraction solid
Cs = solid conc. in solid
Fl = fracture liquid
Cl = solute conc. in liquid

Egn. 3 $$d(F_s C_s) + d(f_\ell C_\ell) = 0$$

Egn. 4 $$\frac{dC_\ell}{(1-k_o)C_\ell} = \frac{df_s}{1-f_s(1-k_o)}$$

Now Cs = Ko Cl, where Ko = Cs/Cl, the equilibrium distribution coefficient Ko is the ratio of the Cs and its equilibrium Cl. In many systems Ko is a function of temperature because the solidus and liquidus lines are curved. In the Al-Cu system these lines are nearly straight and Ko is constant over a wide range of temperatures. Now $dC_s = K_o\, dCl$, and for all fracctions solidfied, Fs = 1-fl.

Eng. 5 $$\frac{C_\ell}{C_o} = \frac{1}{1-(1-k_o)F_s}$$

For a 6.3 Cu alloy we can calculate the fraction solidified prior to the production of eutectic. (at the eutectic Cl = 33.2% Cu).

Egn. 6 $$F_s = \left(\frac{C_o}{C_\ell} - 1\right) / (1 - k_o)$$

or Fs = 0.975. Thus the weight fraction of eutectic is 0.025. This behavior is shown in solidification path 1 in Figure 2. A schematic depicting the conservation of solute for this "equilibrium solidification" is shown in Figure 2. Note that the dearth of solute in the solid is exactly equal to the excess solute in the liquid at all f_s. Note further that dCs/dx and dCℓ/dx are both zero. Equilibrium of the sort described above does not occur in nature, particularly not in welds. The heat of fusion that must continually be dissipated to the surroundings prevent attainment of equilibrium, but the redistribution of solute required in both the solid and liquid poses an even greater obstacle. Because adjustments to the solid composition can occur only by diffusion, the adjustment is sluggish and limiting. Postulating no diffusion in the solid, but complete mixing in the liquid $(dC/dt)x = 0$ in solid, $(dc/dx)x = 0$ in liquid), we can calculate a corrected volume of eutectic. Equilibrium is still maintained, but only at the microscopic level. In regions a few atoms thick on either side of the solid-liquid interface free energy is minimized if C_s and C_L are as predicted by the phase diagram. The behavior of a 6.3% Cu alloy, solidifying under these constraints, is shown as 2 in Figure 2. Notice that the average composition of the solid, at any temperature, is intermediate to the solid in equilibrium with liquid of nominal composition and the solid composition at the interface, C_s^*. Assuming a rectangular volume of liquid with unit cross section, solidifying by the passage of a planar front

Egn. 7 $$(C_L - C_S^*)\, dF_s = (1 - F_s)\, dC_L$$

or

Egn. 8 $$(C_\ell - k_o C_\ell)\, dF_s = (1 - F_s)\, dC_\ell$$

therefore

Egn. 9 $$\frac{dF_s}{(1 - F_s)} = \frac{dC_\ell}{C_\ell (1 - k_o)}$$

PERTINENT SOLIDIFICATION THEORY

Equilibrium Solidification

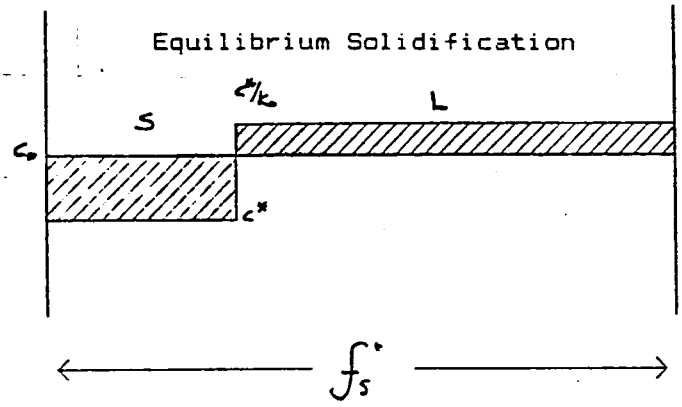

$C_\ell / C_o = \{ 1 - (1-k_o) F_s$

Complete Mixing both S,L

Non-Equilibrium Solidification

$C_\ell / C_o = (1-F_s)^{(k_o-1)}$

$(dC/dt)_{x,s} = 0 \quad (dC/dx)_\ell = 0$

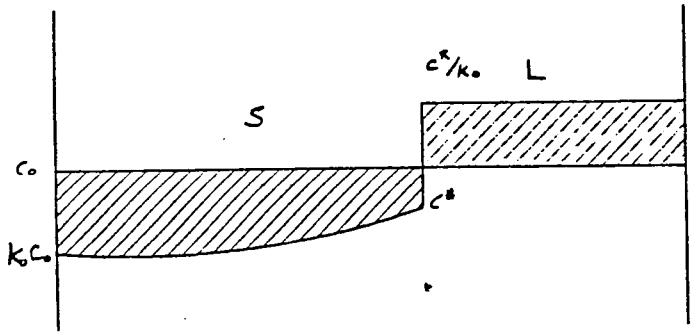

Steady State Solidification

$C_\ell / C_o = \{1+[(1-k_o)/k_o] e^{(-RX/D)}$

$(dC/dt)_{x,s} = 0$ Diffusive Mixing in L

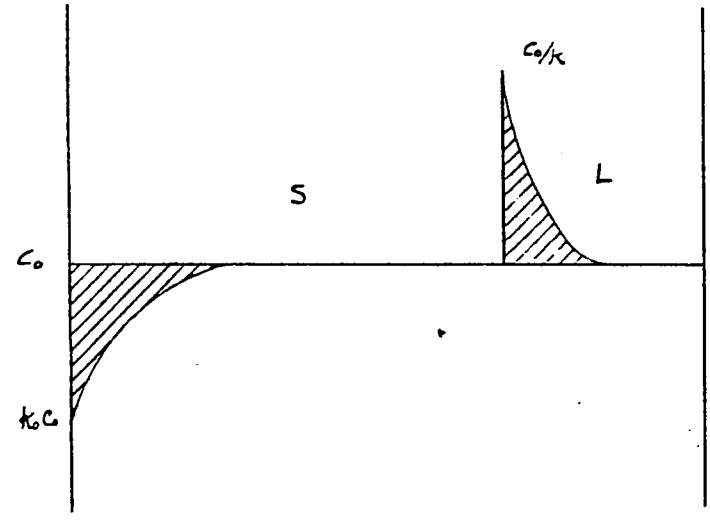

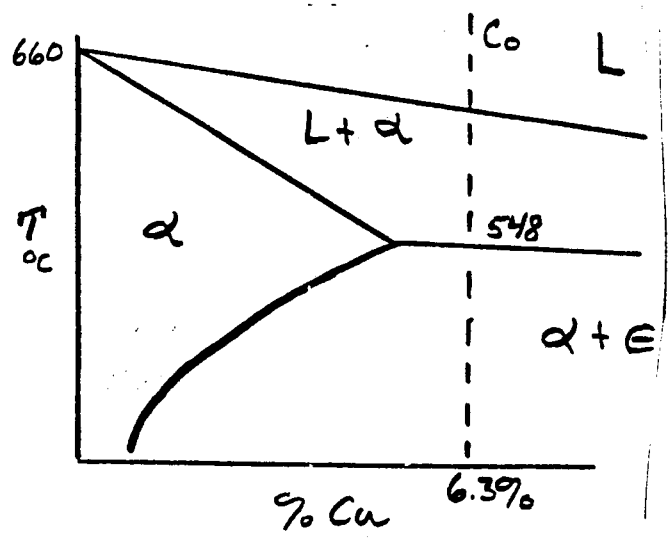

Figure 2.

Integrating we find

Egn. 10 $$-\ln(1-F_s) = \frac{1}{(1-k_o)} \ln \frac{C_e}{C_o}$$

thus

Egn. 11 $$C_e = (1-F_s)^{(k_o-1)} C_o$$

but $C_s^* = k_o C_e$

and

Egn. 12 $$C_s^* = k_o C_o (1-f_s)^{k_o-1}$$

This behavior yields 0.13 volume fraction of eutectic, much more than under equilibrium conditions. The increase is caused by the change in the solute distribution in the solid. Figure 2 shows this effect schematically. Composition is shown as a function of distance (which corresponds to volume fraction). More eutectic forms because the initial solidified cell composition, and thus the average composition when the eutectic starts to form is less than under equilibrium conditions.

Steady state solidification can be produced by assuming diffusive mixing in the liquid. Given a rectangular volume of unit cross section, subject to defussive flux the change in concentration in any differential volume as a function of time can be calculated. If two planes are separated by dx the flux into the volume, across the first plane is

Egn. 13 $$J_1 = -D\left(\frac{dc}{dx}\right)_1$$

and the flux across the second is

Egn. 14 $$J_2 = -D\left(\frac{dc}{dx}\right)_2$$

and the net flux can be found as the difference between J_1 or J_2.

Egn. 15 $$\text{Now } \left(\frac{dc}{dx}\right)_2 = \left(\frac{dc}{dx}\right)_1 + \left(\frac{\partial^2 c}{dx^2}\right) dx$$

thus

Egn. 16 $$J_{net} = D\left(\frac{\partial^2 C}{\partial x^2}\right) dx$$

Egn. 17 $$J_{net}/\partial x = dC/dt$$

Egn. 18 $$dC/dt = D\, \partial^2 C/\partial x^2$$

It is instructive to examine a rectangular volume, solidifying from one end, Figure 2. Solidification in this case is subject to the constraints that $dC/dt = 0$ or that there is diffusive mixing in the liquid. The first solid to form has composition $K_o C_o$. The remaining liquid is enriched in solute ($K_o C_o < C_o$). Because there is no mechanical mixing in the liquid a solute concentration gradient is developed in the liquid adjacent to the solidifying interface. Again, at all times solute is conserved. The loss of solute in the solid corresponds to the solute gain in the liquid. As shown previously the loss of solute from a volume element in the gradient region is

Egn. 19 $$J_D = D\,\frac{\partial^2 C}{\partial x^2}$$

However, the moving interface sweeps up solute, and the flux by interface migration is

Egn. 20 $$J_m = R\,\frac{dC}{\partial x}$$ R = rate of solidification

When C_L at the interface reaches C_o/K_o a condition of dynamic stability is established and

Egn. 21 $$R\,\frac{dC}{\partial x} + D\,\frac{\partial^2 C}{\partial x^2} = 0$$

This equation has a solution of the form

Egn. 22 $$C_d = C' e^{-(R/D)x} + C_o$$

where $$C' = \frac{C_o}{K_o} - C_o = C_o\left(\frac{1-K_o}{K_o}\right)$$

and X' = distance ahead of the solid-liquid interface

thus

Egn. 23 $$C_d = C_o\left[1 - \left(\frac{1-K_o}{K_o}\right) e^{-(R/D)x'}\right]$$

Materials and Procedures

The experimental portion of this study was comprised by two major programs:

1) Determination of the events that lead to the formation of linear enigmas in Al-2219 VPPA welds.

2) Determination of the electrical character of the VPPA arc during the straight polarity portion of the cycle vis-a-vis the reverse segment.

In the enigma program, several series of welds were made. First, a group of modified production welds were made on 0.500 inch thick, 10" x 24" aluminum 2219 plates. Each plate was welded in the vertical position, using a production schedule for plates of this thickness to make bead on plate welds. The first pass was a fully penetrating keyhole 20" long. the second (fill) pass was made, terminating 1" prior to the root pass. Six subsequent autogenous passes were made, the next two terminating after 14" of weld, the final four after 9" of weld. Three plates of this type were made, one with standard production parameters, one with the same parameters, but a 15ms/8ms straight/reverse cycle (vis-a-vis the typical 19ms/4ms), and one with increased torch standoff. Each weld was sectioned to provide samples from each region for optical microcopy, scanning electron microscopy, and radiography. Samples examined in the x-ray were wrapped in lead to minimize anomalous surface effects (backscatter). Plate sections were also characterized using the Computer Aided Tomography system. A fourth plate was welded using the parameters for the first plate. However, instead of overlaying the cover passes, each subsequent pass was moved over one half bead width, (alternating sides) producing a "Nydra" like effect.

Several welds were made while using the UV Nitrogen Laser Vision system to record the appearance of the posterior of the keyhole. These welds were made in 0.375" plate in the vertical position. The weld toe was examined in detail, partial melting and local plate distortion were recorded.

Several stationary VPPA welds were made on 1" thick Al 2219 in the vertical position. Three different arc durations were used, one, tow, and five minutes. These welds were examined with stereography and scanning electron microscopy. Finally, several two pass welds were made on 0.500 inch plate while the plate was clamped in a vise. This clamping force put the plate in compression over central region ten inches long. The behavior of the weld was monitored, and several transverse sections were examined using optical microscopy.

During the course of the second program twelve 0.500 inch aluminum 2219 plates were welded, all in the vertical position. In addition four 0.250" Inconel 718 plates were welded, all in the flat position. Table 1 lists the welding parameters used in this program. In the course of the study welding amperage, welding current, plasma gas pressure, standoff, and straight/reverse polarity distribution were varied. Welding voltage and welding current were measured using photographs of stored oscilloscope traces. The welding operation was abruptly terminated to retain a fossil record of the keyhole. The welds were sectional and characterized by both an optical comparator and after polishing an optical microscope. An energraphics plotting routine was used to generate expressions that described weld contour. The weld region was characterized by microhardness transverse.

ESULTS AND DISCUSSION

Enigma Formation

Figure 3 shows the weld compoite zone. A region of complete melting (fusion zone), a partially melted region, and a region where the base metal character is altered only by solid state reaction is evident. Figure 3A contrasts the microstructure of the base metal far removed from the weld and microstructure of the fusion zone. Using equations developed in the introduction, the volume fraction of eutectic constituent is calculated as 2.5% for the bas metal, but 13% for the weld region. These calculated values correspond well with the amount of eutectic seen. Under fully equilibrium conditions, the base metal is composed of the aluminum rich solid solution of Cu in a FCC structure (α) and CuAl2. However, because the 2219 alloy has a complex thermomechanical history, the α phase is super saturated in Cu. The alloy is cold-worked and aged to foster the precipitation of metastable phases on dislocation networks. As the alloy is overaged, metastable phases transform to $CuAl_2$, which grows and becomes visible to optical microscopy. Throuthout the matrix, before overaging, the 2.5% eutectic present is in a divorced morphology. Globlues of $CuAl_2$ appear as a distinct phase in the structure rather than as a eutectic mixture of two phases. The eutectic freezes in a "divorced" fashion because the component freezes epitaxially on the primary α surrounding the eutectic liquid, leaving the tetragonal $CuAl_2$ laves to form terminally.

Figure 4 is a scanning electron micrograph of the as welded surface of the weld crown. The bead surface appearance is remarkably uniform. Figure 5 is an energy dispersive x-ray analysis of region A in Figure 5. Figure 6 is a corresponding analysis of region B. These analysis support the contention that region A is a cellular dendritic alpha region, and region B is a eutectic mixture. The volume fraction of the terminal liquid is significantly more than the the maximum predicted by solidification mechanics. Furthermore, the volume fraction of the eutectic constituent is greater in the weld toe and the partially melted regions, and slightly increased in the crown overlap region. In addition root passes examined showed enrichment in regions where a slight "U" groove was formed between the molten wall and the root pass crown. The largest effect was found in severely crowned beads. Figures 2 and 3 show a weld schematic indicating regions where enigmas are often seen, and indicating mechanisms proposed to account for these indications. These regions were produced using a technique developed by Nunes and Ding[2]. Several physical processes have been touted to account for the macrogregation (excess eutectic) noted in these cases, they are:

STRUCTURE -- RADIOGRAPHY CORRELATION

(1) Fusion Zone
(2) PMZ
(3) Solid State
(4) Toe Region
(5) Overlap PMZ
(6) Base Metal

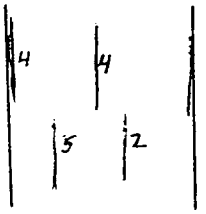

X-ray, Plan View

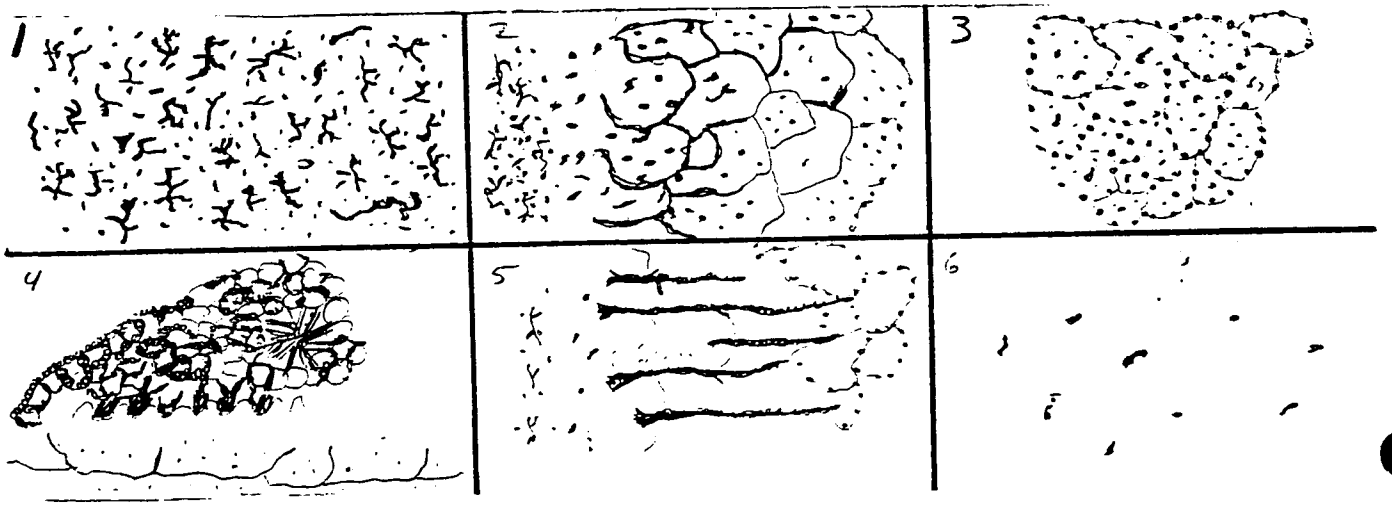

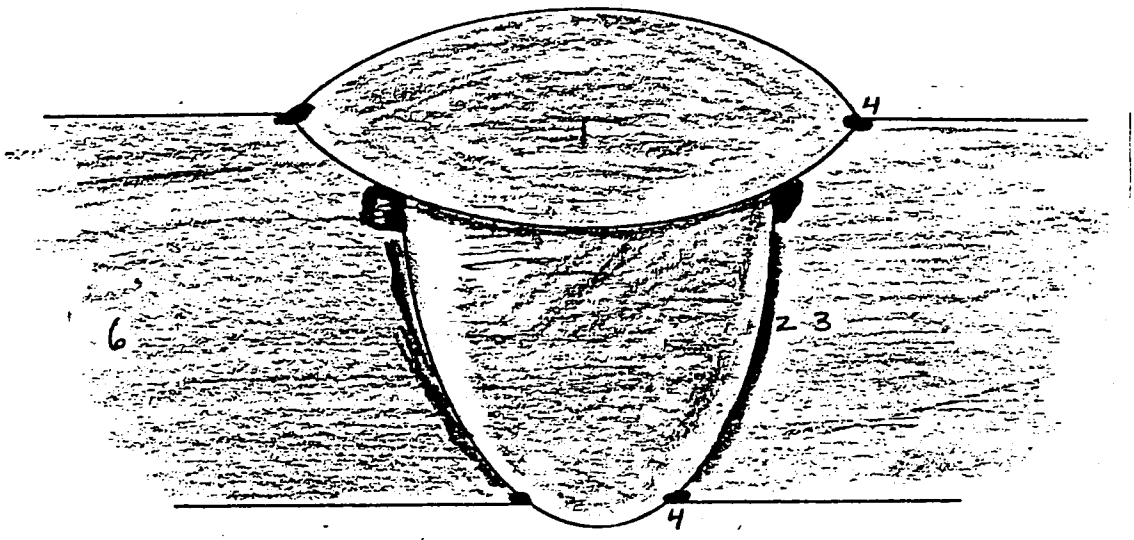

Weld Transverse Cross Section

Shading represents X-ray intensity, microstructures drawn in insets.

Figure 3. Note the distribution of micostructural constituents. Sections 2 and 5 are each located in the PMZ. however region 5 shows back-filled cracks. These cracks are recognized by their size and orientation.

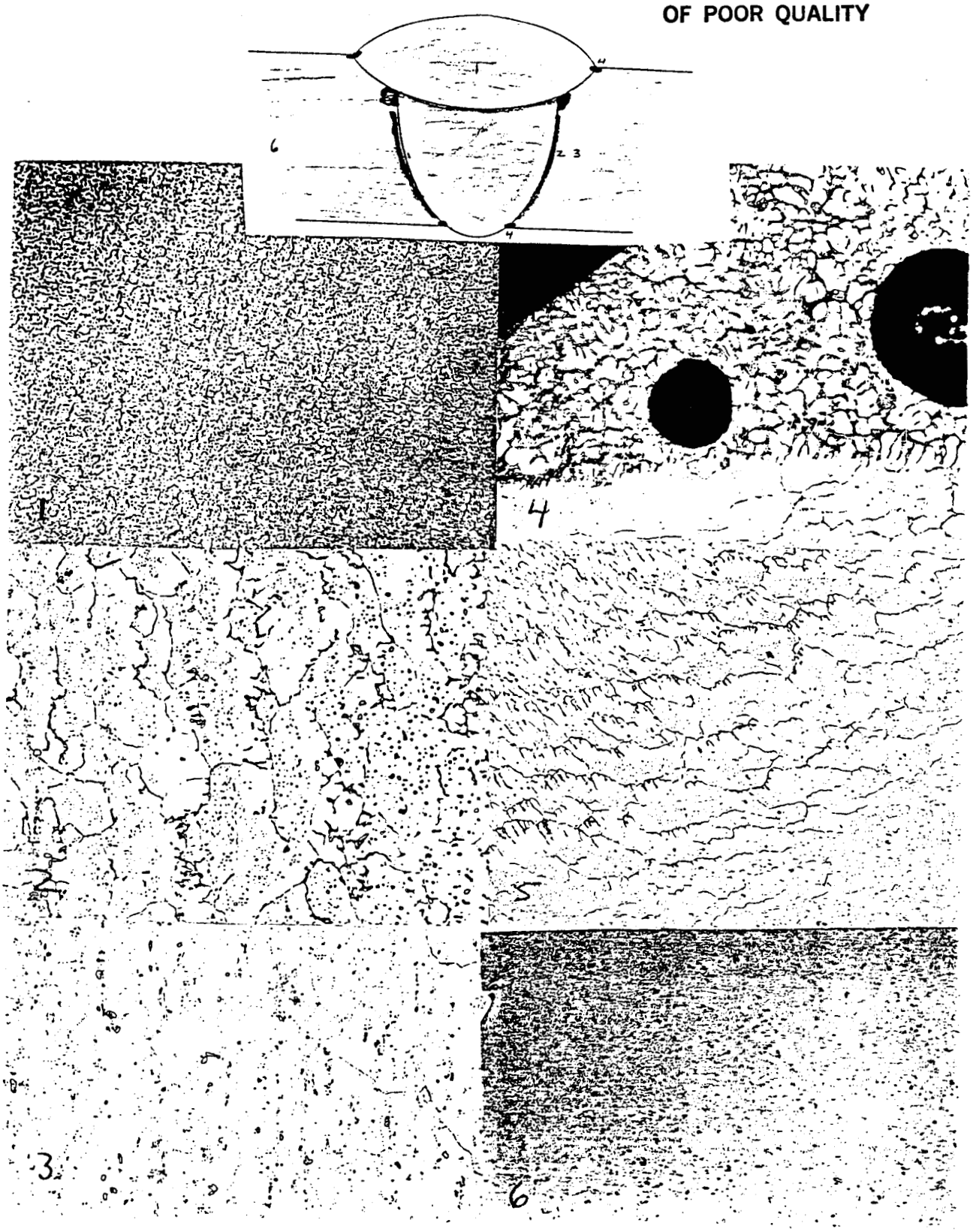

Figure 3a. Actual Microstructures Found in The Regions Indicated

Inverse segregation
Exudation
Preferential Evaporation*
Preferential Sputtering*
Preferential Oxidation*
Solid Bonding
Divorced Eutectic Formation*
High Frequency Effects*

These mechanisms marked by an asterik can also explain copper concentrations in excess of the eutectic observed by some investigators.
Inverse Segregation: Occasionally, solute rejected during solidification is present at higher concentrations in solid regions that form during initial solidification. This can be explained on the basis of volume changes during solidification. Scheil[3] generated an expression for the change in concentration produced by inverse segregation.

Egn. 25 $$\Delta C = C - C_o = \frac{\frac{M_{se} C_{se}}{a_e} + M_{ke} C_{ke}}{\frac{M_{se}}{a_e} + M_{ke}} - C_o$$

(Assuming no pore formation)

C_o = nominal composition
C = mean solute conc. at point
Mse = Mass of liquid/unit length at Cse in liquid
Cse = Solute in liquid at eutectic temperature
Mke = Mass of solid kanit length at Cke in Solid
Cke = Solute conc. at solid interface at Te
Ae = Eutectic solid volume/eutectic liquid volume

Kirkaldy[4] discussed the ramifications of this equation in rigorous mathematical detail. Relations between solute concentrations and solid and liquid densities must be used to evaluate this expression. The loss of solute in the liquid is equal to that gained by the solid (On the basis of total mass, the liquid looses solute, even though the concentration increases). However we must correct for that solute contained in fluid transported into the volume by volume contraction, and that solute transported out of the interdendritic region by contractions in the interdendritic channel. Interestingly, the specific volume of the solid is greater than the specific volume of the liquid for solidifying Al-Cu alloys over a wide range of temperatures. This does not provide a micromechanism for exudation, however, because the specific volume of the liquid decreases as a function of temperature at a rate in excess of the solid specific volume.

The extent of inverse segregation in structures solidifying under near equilibrium and under non-equilibrium conditions can be estimated by selecting appropriate values for the variables in equation 28. Mke can be estimated as the volume fraction of the solid predicted at Te, multiplied by the specific gravity of the mean solute concentration in the cored crystal. Mse can be estimated as the volume fraction of eutectic liquid when Cse is just reached, multiplied by the specific gravity of the liquid. These values can be determined from solidification mecahnics in conjunction with the data of Pourier[5] and Suaerwald[6]. Estimated values are shown in Table 2.

TABLE 2

	Equilibrium	Non-Equilibrium
Mke	2.613	2.218
Mse	0.081	0.416
Cke	0.0565% Cu	0.021% Cu
Cse	0.332% Cu	0.332% Cu
Ce	0.9411	0.9411

ΔC equilibrium = 0.002, (2%)

ΔC nonequilibrium = 0.008, (8%)

These numbers compare favorably with those predicted, and experimentally determined by Kirkaldy[5]. This segregation is not great enough to account for well defined enigmas. Simon and Jones[7] noted that inverse segregation in Al-Cu alloys was more severe in reducing atmospheres.

Figure 4.

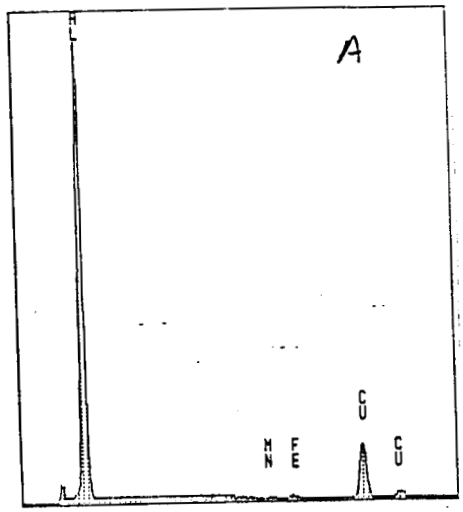

Figure 5.

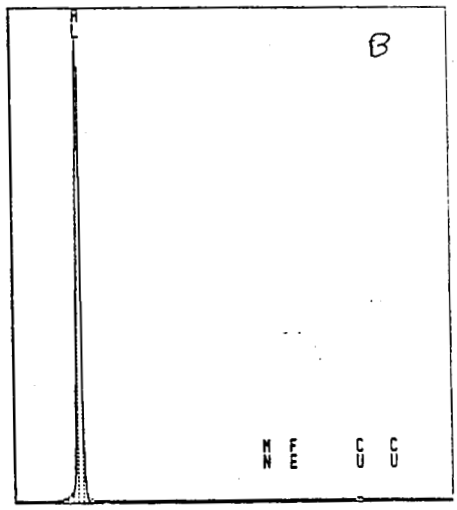

Figure 6.

The quantity D/R can be thought of as a "characteristic distance". At a distance of 5 (D/R) from the interface, less than 1% of the gradient remains. An expression for the "effective distribution coefficient," which takes not only a stagnant diffusive boundary layer, but a bulk mixing effect into account.

Egn. 24 $$k_E = \frac{k_o}{k_o + (1-k_o)\, e^{-(R\delta/D)}}$$

where δ is the boundary layer thickness.

Note, as $\delta \uparrow$ $k_E \rightarrow k_o$

as $R \uparrow$ $k_E \rightarrow k_o$

as the rate of solidification increases the boundary layer thickness required to produce equilibrium solidification decreases.

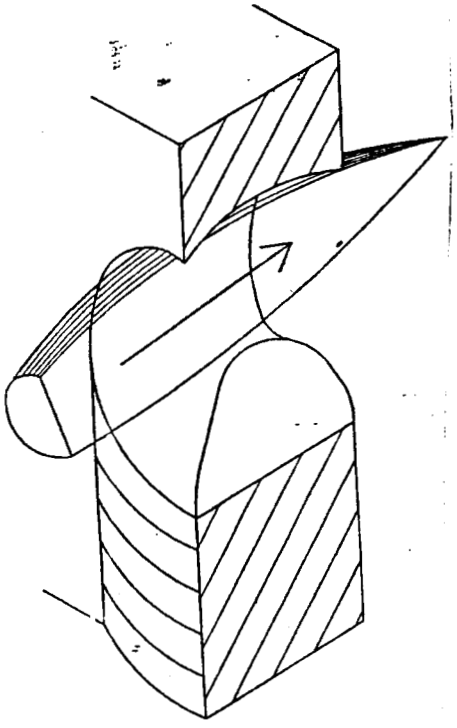

Figure 1. VPPA Keyhole

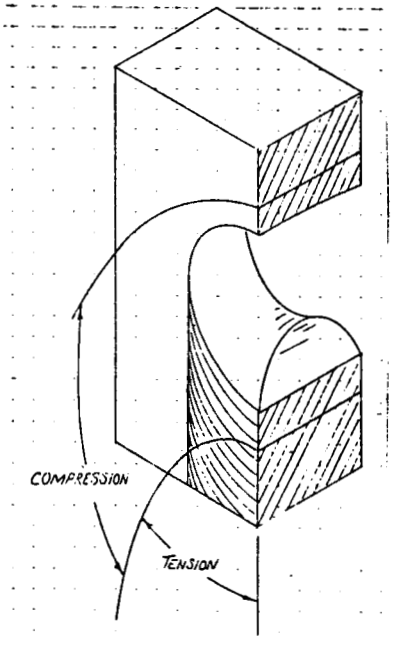

Figure 7. X-Y Stress around Keyhole (a). Exudate at Toe of Weld (b).

Segregation was most severe under atmospheres rich in hydrogen or water vapor. This segregation was related to the formation of gas bubbles as weld solidification progressed. Many small "bubbles" are noted in the toe regions of some welds in Al 2219. Figure 3a shows segregate enrichment near these bubbles. This effect will not produce the type of indication seen in Figure 3, but could lead to periodic x-ray intensity variation.

EXUDATION:

Residual stresses exist in all weld joints. However, the residual stress produced by welding does not influence fluid segregation. Transient stress, associated with the passage of the welding arc is more critical, and can effect solute distribution. Masubushi[8] has demonstrated that compressive stresses exist in the weld region for a brief period before and immediately after the passage of the arc, Figure 7. The compressive stress in the weld region during solidification would promote exudation of enriched liquid from the intercellular regions. Figure 8 depicts the surface regions of a partially melted zone(pmz). Region A is a grain in the pmz, B a region of cellular solidification in prior weld metal and C the intercellular liquid. Elemental analysis in these regions are consistent with non-equilibrium solidification mechanisms proposed to account for the solute distribution and eutectic volume fraction. The intercellular region is typical of the alpha - $CuAl_2$ eutictic composition. Mn and Fe have also segregated to this region. Figure 3 depicts the typical structure of the eutectic. The arrow indicates a long needle, with a morphology typical of the more complex Cu-Al-Fe-Mn phase. The analysis of the solidified cell indicates a copper content lower than that found in the fluid encircled parent gain in the pmz. Cs in the cell can be estimated as 2.1% copper. That of the grain, subject to the theromomechanical history of the Al-2219 parent plate is near 5%. This is shown schemetically in Figure 14. The eutectic intercellular constituent is in relief at the weld surface, toe, and PMZ regions consistent with the compressive stress in these regions during welding.

Another effect based on a coupling of chemical segregation and mechanical stress is the enrinchert noted in the "double" HAZ region. Nunes[9] constructed a mathematical model of microfissuring in Inconel 718 welds. The model is based on an accumulated critical fracture strain. Interestingly, where Masubuchi relegates stress in the through plate (Z) direction to be zero in his transient stress calculation, Nunes assumes this to be the critical feature in microfissuring. This assumption was based on a study of crack morphology. The preponderance

of observed flaws indicate that the stress responsible for microfissuring is oriented perpendicular to the work piece. Figure 3 schematically depicts a common enigma found by transverse x-ray examination. This region is analogous, in two pass VPPA welds, to the hot-crack danger region found by Nunes. Figure 3 depicts this region in VPPA and GTAW welds in Al-2219. The weld procedure used promoted hot cracking in the base material. Copper enrichment in this region occurs by back filling of microfissures. Alloy 2219 is crack resistant because a large volume of terminal liquid can repair flaws that form. These regions are seen in the figure. A crack forms along the grain boundaries in the PMZ, and enriched liquid from the interface flows into the flaw by capillary action. Cracks are evident because of the directicility and extent of the fluid incursion. Interestingly, this leaves a depleted region adjacent to the flawed area, exactly what is noted on radiographs. Savage and Dix[10] have described elemental distributions in back filled flaws.

Vaporization

Vapor is generated from the pool and surrounding environment during welding. The constitution of the vapor will not reflect that of the melt, higher vapor pressure components will be over-representated in the vapor[11]. In a 2219 weld, the major constituent of the vapor is aluminum, whereas in a 2014 material Zn and Mg will be present. The minor alloy components have a great effect on the maximum pool temperature.

For a pure material

Egn. 26 $$\Delta G^{\circ}_{e} = -RT \ln P^{\circ}_{a}$$

by the Clausius-Clapeyron Equation

Egn. 27 $$\frac{dP}{dT} = \frac{S_v - S_l}{V_v - V_l}$$

or

Egn 28 $$\frac{dP}{dT} = \frac{\Delta H_v}{T(V_v - V_l)}$$

therefore

Egn. 29 $$\log \frac{P_2}{P_1} = \frac{\Delta H_v \ (T_2 - T_1)}{2.303 \ R(T_2 - T_1)}$$

To extend the treatment to vapor loss from the solid, we need only to replace ΔH_v with ΔH_s, the heat of sublimation. Typically $\Delta H_s = (1.1)\ \Delta H_v$ H_v. For an alloyed material, the free energy change becomes

Egn. 30 $$\Delta G_e^\circ = \Delta \bar{G}_A$$

but

Egn. 31 $$\Delta \bar{G}_A = -RT \ln \bar{P}_a$$

$$\therefore \Delta G^\circ_{Tot} = RT \ln \bar{P}_a / P_a^\circ = RT \ln a_a$$

The relation can be used to calculate the equilibrium pressure of a species as a function of temperature. Dushman and Laferty[12] and Matsuda[13] have predicted the rate of material loss from the surface as

Egn. 32 $$\gamma_a = 44.3\ P_a \left(M/T\right)^{1/2}$$

for aluminum pools the maximum is approximately 10^{-4}g/scm^2. The maximum loss from a stationary fluid region at the weld toe is $\approx$ 10^{-5}g/SCM^2, and that in the solid regions adjacent to the toe is $\approx$ 10^{-7}g/SCM^2. A 1 cm^2 surface of aluminum in the partially melted region will lose

$$\left(10^{-7}\ g/s\,cm^2\right)\left(27\ g/1\ mole\right)^{-1}\left(\frac{6.02\times10^{23}\ AT}{mole}\right)$$

or

$$\approx 10^{15}\ atoms/s\,cm^2$$

Because the surface exposes 6.25 x 10^{14} atoms/cm^2, it will lose 2 to 10 layers per second. The surface is exposed to temperatures in the range discussed for 5 seconds. Thus it will loose 10 - 50 atom layers of aluminum. This is enough enrichment to be seen in Edax or Auger examination. Further surface enrichment is caused by sputtering. When a neutral atom or a charged species strikes a surface and causes a neutral atom to be removed for that surface the surface is said to be sputtered. Pattee[14] et al have shown that this occurs only under the arc region during reverse polarity segments in plasma welding. Argon atoms sputter

2219 efficiently, but Heliium does not. Therefore Argon is used as the plasma gas because it removes arc-disrupting, rectifying layers of aluminum oxide from the work surface. Sputtering action removes aluminum with greater efficiency than it removes copper, owing to the mass of target atoms. The greater affinity of aluminum for oxygen will also promote a copper enrichment at the surface. Stationary VPPA welds made on a vertical surface were examined by optical and scanning electron microscopy. Large volumes of eutectic liquid have formed on the surface of the bead. These are accumulated volumes of eutectic liquid. Elemental analysis in these regions did occasionally indicate concentrations of copper in excess of the eutectic.

Several authors[15] have advanced solute banding, promoted by velocity changes in the pool, as a mechanism for weld toe solute enrichment. Though it is true that rich solute bands are formed, and that their frequency is greater at the pool edge, so too are solute poor bands formed and their frequency is greater at the edge. There is no net effect on solute produced.

In summary, enigmas are produced by the action of microsegregations mechanisms intimately related to all welding processes. When coupled with the mechanical stress state near the pool, these mechanisms can produce exaggerated conccentration of copper in well defined areas. Further concentration of copper in crown toe area can occur by evaporation, sputtering, and oxidation. Root toe areas are formed by a similar mechanism, but no further enrichment by sputtering can occur.

Arc Characterization

The measured amperage and voltage, for the range of conditions studied is shown in Table 1. In aluminum a rise in voltage of $\approx$ 8V is encountered on switching to reverse polarity, Figure 9. In both straight and reverse polarity the voltage increases as standoff increased. The amperage associated with the straight polarity portion of the cycle increased so as to provide a time averaged current that approximates the program current. It does not, however, average power.

Figure 8. The Partially Melted Zone (PMZ).

Table 1.

ORIGINAL PAGE IS
OF POOR QUALITY

Plate	Amperage S	Amperage R	Voltage S	Voltage R	Polarity	Standoff	Gas Flow	Current
M1	270	225	38	45	19/4	0.180	8.1	260
M3	275	220	42	51	19/4	0.250	8.1	260
M5	270	225	35	43	19/4	0.110	8.1	260
M7	280	225	38	53	19/4	0.180	10.1	260
M9	290	230	37	51	19/4	0.180	5.1	260
M11	300	215	38	47	15/8	0.180	8.1	260
M13	240	185	38	46	15/8	0.180	8.1	210
M15	330	235	45	52	15/8	0.180	8.1	290
M17	280	210	43	52	15/8	0.250	8.1	260
M19	275	230	34	43	15/8	0.110	8.1	260
M23	315	230	37	47	12/12	0.180	8.1	260
M27	270	225	34	42	19/4	0.180	8.1	260

R= reverse cycle S= straight cycle current in amps, potential in volts, standoff in inches, gas flow in cfh.

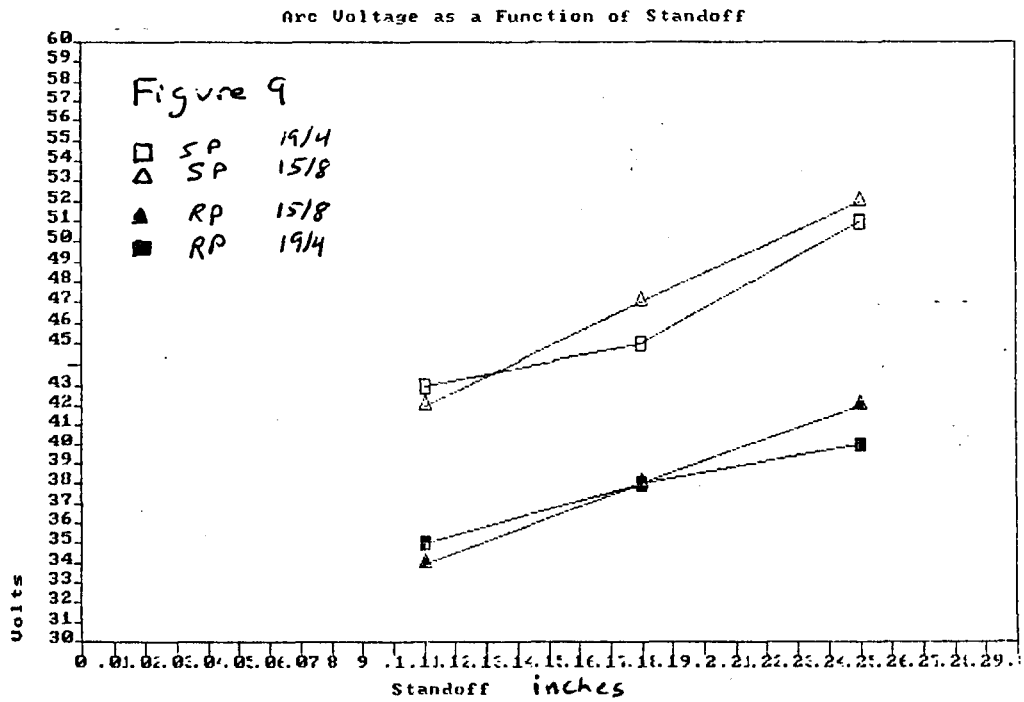

APPENDIX I

Historical Perspective - Alloy 2219

Aluminum alloy 2219 was initially examined as a candidate for spacecraft applications in March of 1962; during the SATURN program. Designers were well aware that the performance of high strength aluminum structures were limited by the characteristics of the weld joints in these materials. Despite their inherent problems, Al-Cu alloys were desirable because of favorable strength to weight ratios and the lack of a low temperature ductility transition. The former attribute provides weight savings in structural applications, the latter makes Al-2219 the aluminum alloy with the greatest range of service temperature. Aluminum 2219 is basically a binary Al-Cu, age hardening material. Its predecessors, 2014 and 2024 are Al-Cu materials with substantial Mg and Zn added to enhance aging kineties at low temperatures. Alloy 2219, heat treated in equivalent fashion is not as strong as 2024 or 2014 at low temperatures, but has superior high temperature strength as well as superior weldability. Improved weldability is won by increased copper content in the alloy. Compositions of Alloy 2014, 2024 and 2219 are shown in Table A1. Enhanced weldability is caused by an increased volume fraction of liquid during critical periods of solidification. The increase in high-temperature strength is caused by three factors:

1) Alloy 2219 is age hardened with a precipitates. The kinetics of formation of this phase are sluggish vis-a-vis the S' and S Al-Cu-Mg precipitates that strengthen 2014 and 2024. Mg reacts strongly with vacancies and accelerates nucleation of precipitates. S' forms rapidly during natural aging and overages quickly at elevated temperatures.

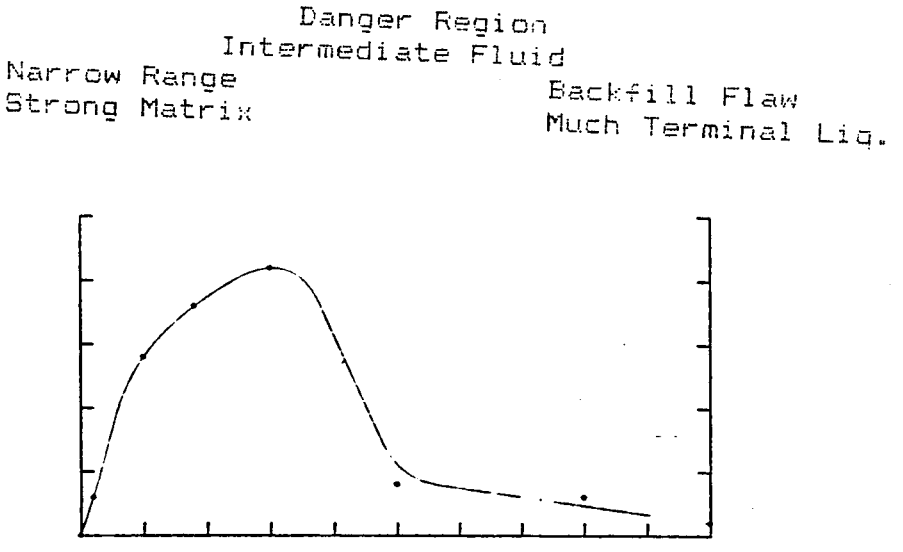

FIGURE A1

2) Mn, Fe, Zr, Ti, and V are present in Alloy 2219. These elements, though present at low concentrations, raise the re-crystallization temperature markedly, and help to pin grain boundaries.

3) The increased fraction of second phase constituents at the grain boundary, caused by increased copper, help prevent the onset of grain boundary sliding.

Aluminum alloy 2219 is used to fabricate the Space Shuttle Main Tank primarily because of weldability considerations. Further, a large data base of cryogenic applications has accumulated since 1962. Alloy 2219 has been used in aircraft parts and structures subject to elevated temperatures as well, therefore the mechanical properties are well understood.

Weldability of Al-Cu Alloys

Two major weldability concerns, with precipitation hardend aluminum alloys, are their susceptibility to hot cracking and their drastic reduction in weld composite region strength. Jennings and Pumphrey[16] did extensive empirical work treating the weldability of binary aluminum alloys. This work was critical to Borlands[17] classic discussion of hot cracking. In all cases hot cracking is predicated on a stress developed across liquid bridges between adjacent solid regions. These stresses can be produced by solidification shrinkage of weld metal in concert with thermal contraction of the workpiece Material with a continuous liquid network along grain boundaries is still capable of supporting loads. Grotke[18] has shown that the strength is related to the film thickness.

Egn A1 $$\sigma = \frac{2\gamma_L}{h}$$

Even with a continuous liquid 750°A thick in the boundry, the material can support a load of 5 ksi. The hot cracking sensitivity of aluminum alloys is critically dependent on the weld metal chemistry. Pumphry[19] has shown that the crack sensitivity of an Al-Cu alloy increases to a maximum near a nominal Cu content of just less than 4% Cu, and then falls to a minimum level near 6% Cu, Figure A1. Borland explains this behavior by postulating a temperature range during solidification during which there is a coherent, load carrying, cellular matrix woven through a liquid that remains to solidify. The material is of low strength and minimal ductility in the temperature range coherency and the solidus. The wider the temperature range between coherency and the final solidification, the greater the tendency to hot crack, because total strain will be directly related to the solidification interval.

If sufficient liquid is present during the latter stages of solidification, incipient cracks that form may be refilled by capillary action. The liquid eutectic, because it freezes at a constant temperature, is the most effective regenerating fluid. Conversely, a dearth of eutectic may aggravate cracking by creating zones of weakness in an interdendritic film. Jenning[16], postulated that maximum cracking occurs at an alloy composition with the greatest range between the solidus on the liquids (the maximum solid solubility). However, the solidification of welds is a non-equilibrium process. Constitutional supercooling greatly changes the volume of terminal eutectic phase produced, and depresses the coherence temperature. Maximum weld cracking occurs at lower copper concentrations that predicted for equilibrium.

To summarize:

1) At low Cu levels, the amount of eutectic terminal transient is not sufficient to form a continuous grain-boundary network. The fraction solidified is large even at slight undercoolings, and the solid forms a strong, crack-resistant network.

2) At intermediate Cu concentrations, the volume of eutectic fluid becomes just sufficient to form a continuous interdendritic liquid, and the crack sensitivity is large.

3) At Cu concentrations near that found in alloy 2219 crack resistance is large. Because the solidification range is diminished, minimizing shrinkage strains, and because the volume fraction of eutectic is sufficient to "back-fill" cracks as they form.

Table A1. Composition of Common Al Alloys

Alloy	Al	Cu	Mn	Mg	Si	V	Zr	Ti
2219	93	6.3	0.3	-	0.8	0.1	0.2	0.1
2014	93.5	4.4	0.8	0.5	-	-	-	-
2024	93.5	4.4	0.6	1.5	-	-	-	-
5456	93.9	-	0.8	5.1	-	(0.12 Cr)		-

Conclusions and Recommendations

- Alloy 2219 is a uniquely weldable binary alloy of aluminum and copper. It is weldable because large volumes of liquid are available during its latter stages of solidification.

- Transient stresses in the weld region produce macrosegregation by causing exudation and by causing flaws that are subsequently back filled. These are the major mechanisms for producing macrosegregation in Al-2219 welds.

- Apparent enrichment, beyond the eutectic composition was found at the weld surface. Sputtering and evaporation can account for this increase.

- Radiographic contrast effects, including the straight line indication (but not diffraction effects) are a result of transient stress induced macrosegregation.

- Contrary to conventional wisdom, more heat is delivered to aluminum, steel, and inconel materials during the reverse polarity portion of the VPPA welding cycle than during the straight polarity segment.

- Current in the welding arc falls during the reverse polarity portion of the welding cycle, but voltage increases. The voltage increases so much that greater power is often produced in the reverse cycle.

- At any programmed current the current in the straight polarity portion of the cycle increases as the proportion of reverse polarity increases.

REFERENCES

1) Walsh, D.W. Summer Report "Physics of the VPPA Weld Keyhole Region; Pool Flows" NASA-ASEE Summer Faculty Program, August 1987

2) Nunes, A.C. Jr., and Ding, J., Private Discussions, Pending Publication, July 1988.

3) Schiel,E., Metallforschung, 1947, V2,p69.

4)Kirkaldy, J.S.anf Youlodis,W.V., "Contributions to the Theory of Inverse Segregation" Met. Trans. 212, Dec. 1958.

5) Pourie, and Ganescu, "Densities of Al Rich Al-Cu Alloys During Solidification" Met. Trans. A 18 Apr. 1988

6) Suarerwals, F. Metallwritschaft, 1943, V22, p543.

7) Adams, D.E., "Segregation in Al-Cu Alloys" J. Inst of Metals 75 1949 p809

8) Masubuchi, K. and Simmons, F. "Analysis of Thermal Stress and Metal Movement During Welding" Redstone Rep. RSIC-820 July 1968.

9) Nunes, AC, "Microfissuring in IN718" NASA TM-82531 June 1983.

10) Savage and Dickinson, "Electron Microanalysis of Backfilled Hot Cracks in Inconel 600. WJ 11, 1972, p543.

11) Block-Boulton and Eagar, "Selective Evaporation of Metal From Weld Pools" Trends in Welding Research, Conf. Proc. ASM 1981

12) Dushman and Laferty, Scientific Foundations of Vacuum Technique John Wiley 1962 p696.

13) Matsuda and Hashimoto, "Penetration Mechanisms in EB Welds" Trans. Nat. Res. Inst. for Metals (Jap.) V7, 5 1965

14) Pattee Meister and Monroe, " Cathodic Cleaning and Plasma Arc Welding of Aluminum" Welding Journal, May 1968.

15) D' Anessa, M.J., "Solute Redistribution in the Weld Pool" Welding Journal, May 1966.

16) Jennings, Singer, and Pumphrey, Journal of the Institute of Metals, 74, 227, 1948 "Hot Shortness of Some High Purity Alloys in the Al-Cu System"

17) Borland, J., British WJ 7, 508, 1960. "Supersolidus Cracking"

18) Grotke, P., "Physical Metallurgy of Hot-Ductility Testing" Welding Journal, Nov. 1970.

19) Pumphrey and Lyons, J. Institute of Metals, 74, 439, 1948 "Cracking During the Welding of the More Common Binary Aluminum Alloys".